Experimental performance of DWDM quadruple Vernier racetrack resonators

Robert Boeck,[*] Jonas Flueckiger, Lukas Chrostowski, and Nicolas A. F. Jaeger

Department of Electrical and Computer Engineering, University of British Columbia, Vancouver, BC, Canada

[*]rboeck@ieee.org

Abstract: We demonstrate that one can meet numerous commercial requirements for filters used in dense wavelength-division multiplexing applications using quadruple Vernier racetrack resonators in the silicon-on-insulator platform. Experimental performance shows a ripple of 0.2 dB, an interstitial peak suppression of 39.7 dB, an adjacent channel isolation of 37.2 dB, an express channel isolation of 10.2 dB, and a free spectral range of 37.52 nm.

OCIS codes: (230.7408) Wavelength filtering devices; (230.5750) Resonators.

References and links

1. O. Schwelb, "The nature of spurious mode suppression in extended FSR microring multiplexers," Opt. Commun. **271**, 424–429 (2007).
2. O. Schwelb and I. Frigyes, "Vernier operation of series-coupled optical microring resonator filters," Micro. Optical Tech. Lett. **39**, 257–261 (2003).
3. Y. Goebuchi, T. Kato, and Y. Kokubun, "Optimum arrangement of high-order series-coupled microring resonator for crosstalk reduction," Jpn. J. Appl. Phys. **45**, 5769–5774 (2006).
4. D. Zhang, Y. Huang, X. Ren, X. Duan, B. Shen, Q. Wang, X. Zhang, and S. Cai, "Add-drop filters based on asymmetric high-order microring resonators," Proc. SPIE **8555**, 85550U-1–85550U-7 (2012).
5. S. Dey and S. Mandal, "Modeling and analysis of quadruple optical ring resonator performance as optical filter using Vernier principle," Opt. Commun. **285**, 439–446 (2012).
6. C. Chaichuay, P. P. Yupapin, and P. Saeung, "The serially coupled multiple ring resonator filters and Vernier effect," Opt. Appl. **39**, 175 (2009).
7. H. Yan, X. Feng, D. Zhang, and Y. Huang, "Integrated optical add-drop multiplexer based on a compact parent-sub microring-resonator structure," Opt. Commun. **289**, 53–59 (2013).
8. V. M. N. Passaro, B. Troia, and F. De Leonardis, "A generalized approach for design of photonic gas sensors based on Vernier-effect in mid-IR," Sensor. Actuat. B-Chem. **168**, 402–420 (2012).
9. G. Ren, T. Cao, and S. Chen, "Design and analysis of a cascaded microring resonator-based thermo-optical tunable filter with ultralarge free spectrum range and low power consumption," Opt. Eng. **50**, 0746010746016 (2011).
10. F. Boffi, L. Bolla, P. Galli, S. Ghidini, and L. Socci, "Method and device for tunable optical filtering using Vernier effect," U.S. Patent EP2181348 B1 (2012).
11. E. J. Klein, "Densely integrated microring-resonator based components for fiber-to-the-home applications," Ph.D. dissertation, University of Twente (2007).
12. S. Suzuki, K. Oda, and Y. Hibino, "Integrated-optic double-ring resonators with a wide free spectral range of 100 GHz," J. Lightwave Technol. **13**, 1766–1771 (1995).
13. S.-J. Choi, Z. Peng, Q. Yang, S. J. Choi, and P. D. Dapkus, "Tunable narrow linewidth all-buried heterostructure ring resonator filters using Vernier effects," IEEE Photon. Technol. Lett. **17**, 106–108 (2005).
14. S. T. Chu, B. E. Little, V. Van, J. V. Hryniewicz, P. P. Absil, F. G. Johnson, D. Gill, O. King, F. Seiferth, M. Trakalo, and J. Shanton, "Compact full C-band tunable filters for 50 GHz channel spacing based on high order micro-ring resonators," in *Optical Fiber Communication Conference* (Optical Society of America, 2004).

15. T. Chu, N. Fujioka, S. Nakamura, M. Tokushima, and M. Ishizaka, "Compact, low power consumption wavelength tunable laser with silicon photonic-wire waveguide micro-ring resonators," in 35th European Conference On Optical Communication (ECOC), 1–2 (2009).
16. P. Prabhathan, Z. Jing, V. M. Murukeshan, Z. Huijuan, and C. Shiyi, "Discrete and fine wavelength tunable thermo-optic WSS for low power consumption C+L band tunability," IEEE Photon. Technol. Lett. **24**, 152–154 (2012).
17. W. Fegadolli, G. Vargas, X. Wang, F. Valini, L. Barea, J. Oliveira, N. Frateschi, A. Scherer, V. Almeida, and R. Panepucci, "Reconfigurable silicon thermo-optical ring resonator switch based on Vernier effect control," Opt. Express **20**, 14722–14733 (2012).
18. R. Boeck, N. A. F. Jaeger, N. Rouger, and L. Chrostowski, "Series-coupled silicon racetrack resonators and the vernier effect: theory and measurement," Opt. Express **18**, 25151–25157 (2010).
19. R. Boeck, J. Flueckiger, H. Yun, L. Chrostowski, and N. A. F. Jaeger, "High performance Vernier racetrack resonators," Opt. Lett. **37**, 5199–5201 (2012).
20. B. Timotijevic, G. Mashanovich, A. Michaeli, O. Cohen, V. M. N. Passaro, J. Crnjanski, and G. T. Reed, "Tailoring the spectral response of add/drop single and multiple resonators in silicon-on-insulator," Chinese Opt. Lett. **7**, 291–295 (2009).
21. M. Mancinelli, R. Guider, P. Bettotti, M. Masi, M. R. Vanacharla, J. Fedeli, D. V. Thourhout, and L. Pavesi, "Optical characterization of silicon-on-insulator-based single and coupled racetrack resonators," J. Nanophotonics **5**, 051705 (2011).
22. Y. Yanagase, S. Suzuki, Y. Kokubun, and S. T. Chu, "Box-like filter response and expansion of FSR by a vertically triple coupled microring resonator filter," J. Lightwave Technol. **20**, 1525–1529 (2002).
23. Y. Goebuchi, T. Kato, and Y. Kokubun, "Expansion of tuning range of wavelength selective switch using Vernier effect of series coupled microring resonator," in The 18th Annual Meeting of the IEEE Lasers and Electro-Optics Society, 2005. LEOS 2005, 734–735 (2005).
24. K. Oda, N. Takato, and H. Toba, "A wide-FSR waveguide double-ring resonator for optical FDM transmission systems," J. Lightwave Technol. **9**, 728–736 (1991).
25. L. Jin, M. Li, and J.-J. He, "Highly-sensitive silicon-on-insulator sensor based on two cascaded micro-ring resonators with vernier effect," Opt. Commun. **284**, 156–159 (2011).
26. J. Hu and D. Dai, "Cascaded-ring optical sensor with enhanced sensitivity by using suspended Si-nanowires," IEEE Photon. Technol. Lett. **23**, 842–844 (2011).
27. T. Claes, W. Bogaerts, and P. Bienstman, "Experimental characterization of a silicon photonic biosensor consisting of two cascaded ring resonators based on the Vernier-effect and introduction of a curve fitting method for an improved detection limit," Opt. Express, **18**, 22747–22761 (2010).
28. X. Jiang, "Silicon nanowire waveguide sensor based on two cascaded ring resonators," in Asia Communications and Photonics Conference, OSA Technical Digest (online) (Optical Society of America, 2012), paper AS4E.3.
29. "Single channel DWDM (100 GHz)," Alliance Fiber Optic Products, Inc.
30. "Optical add/drop multiplexers 100 GHz OADM (1x2)," Photonics-USA.
31. "Fiber optic dwdm single add/drop device," AOXC Technologies.
32. R. Ding, T. Baehr-Jones, T. Pinguet, J. Li, N. C. Harris, M. Streshinsky, L. He, A. Novack, E.-J. Lim, T.-Y. Liow, H.-G. Teo, G.-Q. Lo, and M. Hochberg, "A silicon platform for high-speed photonics systems," in Optical Fiber Communication Conference, OSA Technical Digest (Optical Society of America, 2012), paper OM2E.6.
33. D. Minoli, *Telecommunications Technology Handbook* (Artech House, 2003).
34. "DWDM and CWDM three port device optical parameter definition and test requirements," Alliance Fiber Optic Products, Inc.
35. R. S. Romaniuk, "Optical fiber transmission with wavelength multiplexing: faster or denser?," **5484**, 19–28 (2004).
36. R.J. Bojko, J. Li, L. He, T. Baehr-Jones, M. Hochberg, and Y. Aida, J. Vac., "Electron beam lithography writing strategies for low loss, high confinement silicon optical waveguides," Sci. Technol. B **29**, 06F309 (2011).
37. "High isolation OADM (100 GHz)," Alliance Fiber Optic Products, Inc.
38. C. Manolatou, M. A. Popovic, P. T. Rakich, T. Barwicz, H. A. Haus, and E. P. Ippen, "Spectral anomalies due to coupling-induced frequency shifts in dielectric coupled-resonator filters," in Optical Fiber Communication Conference, 2004, paper TuD5.
39. P. Prabhathan, V. M. Murukeshan, and J. Zhang, "Optimal detuning combinations in a series coupled silicon micro ring resonator thermo optic-wavelength selective switch," Opt. Eng. **51**, 044604 (2012).
40. S. J. Mason, "Feedback theory-further properties of signal flow graphs," Proc. IRE **44**, 920–926 (1956).

1. Introduction

The Vernier effect has been used extensively in the research community to expand the free spectral range (FSR) in ring resonators, and has been demonstrated both theoretically [1–10] and experimentally [11–28]. Ideally, one would like a box-like drop port spectral response, which

#183816 - $15.00 USD Received 28 Jan 2013; revised 25 Mar 2013; accepted 27 Mar 2013; published 4 Apr 2013

can be achieved using series-coupled ring resonators [22]. Increasing the number of series-coupled rings, allows one to increase the clear window (channel bandwidth) and thus the data rate that the filter can handle. However, to date, no one has experimentally demonstrated the Vernier effect in more than three series-coupled rings and no one has experimentally shown whether series-coupled Vernier ring resonators can be used to meet typical commercial filter requirements. Timotijevic *et al.* [20] demonstrated double Vernier silicon-on-insulator (SOI) series-coupled ring resonators which had an FSR larger than the span of the C-band but minimal interstitial peak suppression (IPS). Fegadolli *et al.* [17] fabricated thermally tunable double Vernier SOI series-coupled ring resonators exhibiting the Vernier effect in the through port and drop port. Mancinelli *et al.* [21] used double Vernier SOI series-coupled resonators that had an extended FSR of 20 nm. Prabhathan *et al.* [16] fabricated double SOI cascaded ring resonators exhibiting the Vernier effect at the drop port for use as a thermally tunable wavelength selective switch. The authors' device had an FSR of approximately 50 nm and a drop port out-of-band extinction greater than 15 dB [16]. However, ring resonators in cascaded configurations only exhibit the Vernier effect in the drop port response and not the through port response [11]. Yanagase *et al.* [22] have shown triple-ring resonators exhibiting the Vernier effect, where the coupling was done vertically and the material used for the waveguides was Ta_2O_5-SiO_2. However, their devices show minimal IPS and their extended FSR was less than the span of the C-band. Also, they do not show the through port responses. Previously published research, both experimental and theoretical, show the benefit (FSR expansion) of using the Vernier effect within series-coupled ring resonators, as compared to the case where each resonator is identical, but minimal research has been done regarding meeting commercial requirements as regards to the IPS (see [3, 4, 10, 19]). Here, we experimentally demonstrate that it is, in fact, possible to meet many commercial requirements when using quadruple SOI series-coupled racetrack resonators exhibiting the Vernier effect including the necessary IPS. The commercial requirements that are met are the drop port ripple (R_{depth}), the drop port adjacent channel isolation (A_{i}), the drop port non-adjacent channel isolation (nA_{i}), and the express channel isolation (EC_{i}). It should be noted that the EC_{i} has the same definition as the through port channel extinction ratio and pass channel residual at express port. The IPS is similar to that of the nA_{i}, however, since our device involves the Vernier effect there are multiple peaks between two dominant resonant peaks and, thus, it is important that the IPS meets the commercial specification for the nA_{i}. The target specifications come from commercial dense wavelength-division multiplexing (DWDM) data sheets [29–31].

2. Theory

A schematic of our quadruple series-coupled racetrack resonators exhibiting the Vernier effect is shown in Fig. 1 which is similar to that found in [2–4] (same arrangement of the resonators but different resonator lengths, field transmission and coupling factors, and propagation loss). Here, L_a, L_b, L_c, and L_d are the total lengths of racetrack resonators a, b, c, and d, respectively. L_y is the length of the straight coupling regions, r is the radius of the racetrack resonators, and L is the length of the straight sections (other than those in the coupling regions) for racetrack resonators c and d. α is the total field loss coefficient for the racetracks resonators. κ_1, κ_2, κ_3, κ_4, and κ_5 are the symmetric (real) point field coupling factors. t_1, t_2, t_3, t_4, and t_5 are the straight through (real) point field transmission factors.

#183816 - $15.00 USD Received 28 Jan 2013; revised 25 Mar 2013; accepted 27 Mar 2013; published 4 Apr 2013

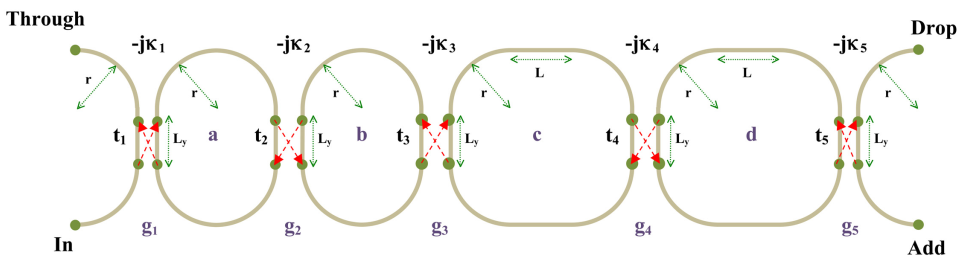

Fig. 1. Schematic of our quadruple series-coupled racetrack resonators exhibiting the Vernier effect.

The following assumptions are made for the design: $L_{a,b} = 2\pi r{+}2L_y$ and $L_{c,d} = (4/3)L_{a,b} = 2\pi r{+}2L{+}2L_y$, where $r = 5\ \mu$m, $L_y = 7\ \mu$m and $L = 7.569\ \mu$m. $\kappa_1 = \kappa_5$, $\kappa_2 = \kappa_4$, $t_1 = t_5$, and $t_2 = t_4$. The waveguides are strip waveguides with a top silicon dioxide cladding having widths and heights of 502 nm and 220 nm, respectively. The propagation loss for each ring was assumed to be 2.4 dB/cm [32]. The modeling and analysis of the quadruple Vernier racetrack resonator was done using a mixture of numeric and analytic methods. Specifically, the effective index of the strip waveguides and the field coupling and transmission factors were determined using MODE Solutions by Lumerical Solutions, Inc., and everything else was done analytically. The gap distances are g_1 = 125 nm, g_2 = 350 nm, g_3 = 410 nm, g_4 = 350 nm, and g_5 =125 nm, respectively. The value of their field coupling and field transmission factors were determined by applying a third order polynomial curve-fit to the wavelength dependent even and odd effective indices. At 1550 nm, the field coupling factors are $\kappa_1 = \kappa_5 = 0.5446$, $\kappa_2 = \kappa_4 = 0.0771$, and $\kappa_3 = 0.0460$ and their slopes are $\mathrm{d}\kappa_1/\mathrm{d}\lambda = \mathrm{d}\kappa_5/\mathrm{d}\lambda = 1.72\times10^{-3}$ [/nm], $\mathrm{d}\kappa_2/\mathrm{d}\lambda = \mathrm{d}\kappa_4/\mathrm{d}\lambda = 4.58\times10^{-4}$ [/nm], $\mathrm{d}\kappa_3/\mathrm{d}\lambda = 3.03\times10^{-4}$ [/nm]. Also at 1550 nm, the effective index is 2.4464 and the slope is -1.12×10^{-3} [/nm]. The theoretical drop port and through port responses are shown in Figs. 2(a) and 2(b). The derivation of the drop port and through port transfer functions can be found in the Appendix. The spectral characteristics are defined based on typical commercial definitions that describe the performance of DWDM filters. We choose a 100 GHz ($\approx$ 0.8 nm) channel spacing and a 6 GHz ($\approx$ 0.048 nm) clear window centered at a desired wavelength (our choice of clear window assumes there will be no laser wavelength drift). The FSR should be greater than or equal to 35.89 nm (the span of the C-band, 1528.77 nm to 1563.86 nm [33], plus one adjacent channel). The definitions for $\mathrm{A_i}$ [34, 35], $\mathrm{nA_i}$ [34, 35], $\mathrm{R_{depth}}$ [33, 34], and $\mathrm{EC_i}$ [34] can be found in the citations given. The spectral characteristics are determined within the clear windows of the desired channel and the 44 clear windows to the left and right of the desired channel. The spectra shown in Fig. 2(a) and 2(b) meet the typical commercial values for the target specifications as shown in Table 1. It should be noted that there is some variance in target values depending on the DWDM vendor. For example, [29] specifies an $\mathrm{EC_i}$ value of 12 dB whereas [30] specifies a value of 10 dB.

#183816 - $15.00 USD Received 28 Jan 2013; revised 25 Mar 2013; accepted 27 Mar 2013; published 4 Apr 2013

Table 1. Theoretical and Target Specifications

Parameter	**Theoretical**	**Target**
FSR (nm)	36.93	$\geq$ 35.89
A_i (dB)	52.7	$\geq$ 25 [29, 30], 30 [31]
nA_i, IPS (dB)	40.4	$\geq$ 35 [31], 40 [29, 30]
R_{depth} (dB)	0.1	$\leq$ 0.5 [30]
EC_i (dB)	11.1	$\geq$ 10 [30], 12 [29]

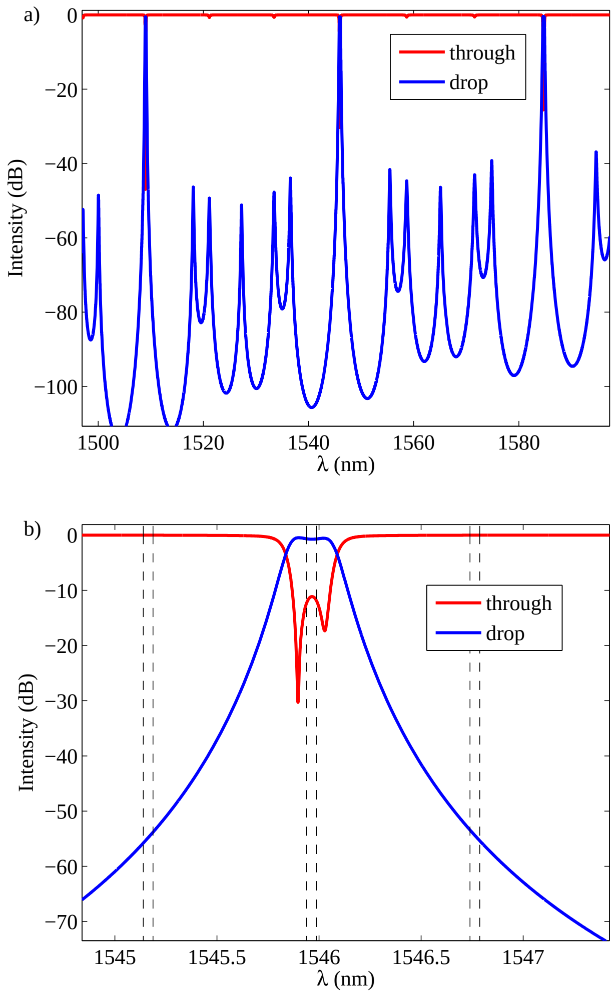

Fig. 2. (a) theoretical spectral response. (b) a "zoom-in" of the major resonance.

#183816 - $15.00 USD Received 28 Jan 2013; revised 25 Mar 2013; accepted 27 Mar 2013; published 4 Apr 2013

3. Fabrication results and discussion

The device was fabricated at the University of Washington using electron beam lithography, as described in [36]. Figures 3(a) and 3(b) show the experimental through port and drop port responses of one of our quadruple Vernier racetrack resonators. Figure 3(a) clearly shows significant IPS. The maximum through port insertion loss (IL_{thru}) [34] and the drop port insertion loss (IL_{drop}) [33–35] have not been included since we were unable to measure them accurately. The spectral characteristics meet numerous commercial requirements as shown in Table 2. The EC_i, R_{depth}, and IPS are within 0.9 dB of the theoretical results. The experimental A_i is 37.2 dB whereas the theoretical A_i is 52.7 dB, which is likely due to the experimental filter line shape being asymmetric and to increased field coupling factors due to the bend regions of the couplers. To be able to simultaneously drop and add signals using just one instance of the device shown in Fig. 1, the target values shown in Table 2 would be needed except that EC_i would need to be greater than or equal to 25 dB [37]. Here, we have defined the IPS as the contrast between the minimum transmission within the clear window of the desired channel and the maximum transmission within the clear windows of all non-adjacent channels. However, it should be noted that in [19], the IPS was defined as the difference (in dB) between the maximum value of a major peak and the maximum value of the largest interstitial peak. Based on this definition, our measured IPS would be 37.1 dB. The much larger notches within the pass band of the through port as compared to the theoretical results are possibly due to fabrication variations and coupling-induced frequency shifts (CIFS) [38, 39], which can be corrected by thermally tuning each racetrack resonator [39]. However, the notches are not located within any of the adjacent or non-adjacent channels as shown in Figs. 3(c) and 3(d). The passband of the through port to the left of the major peak shows that there are actually 4 notches (two small notches and two large notches) as shown in Fig. 3(c). However, our theoretical results showed that there are only two small notches as shown in Fig. 2(a). The likely reasons for this difference between the theory and experimental results are fabrication variations, in which the effective indices of the resonators are not all exactly the same, and CIFS. For example, if the effective index of racetrack resonator a is decreased by 0.003 (as shown in Fig. 3(e)) each of the notches separates into 2 notches (one small and one large), where the larger notch is located to the right of the smaller notch (as shown in Fig. 3(f)), which is in agreement with the experimental results. In addition to the device presented here, we fabricated 48 other devices in which the gap distances were varied. The device presented here showed the best performance. However, future designs based on this device can be made to be thermally tunable to compensate for fabrication variations and effects such as CIFS.

#183816 - $15.00 USD Received 28 Jan 2013; revised 25 Mar 2013; accepted 27 Mar 2013; published 4 Apr 2013

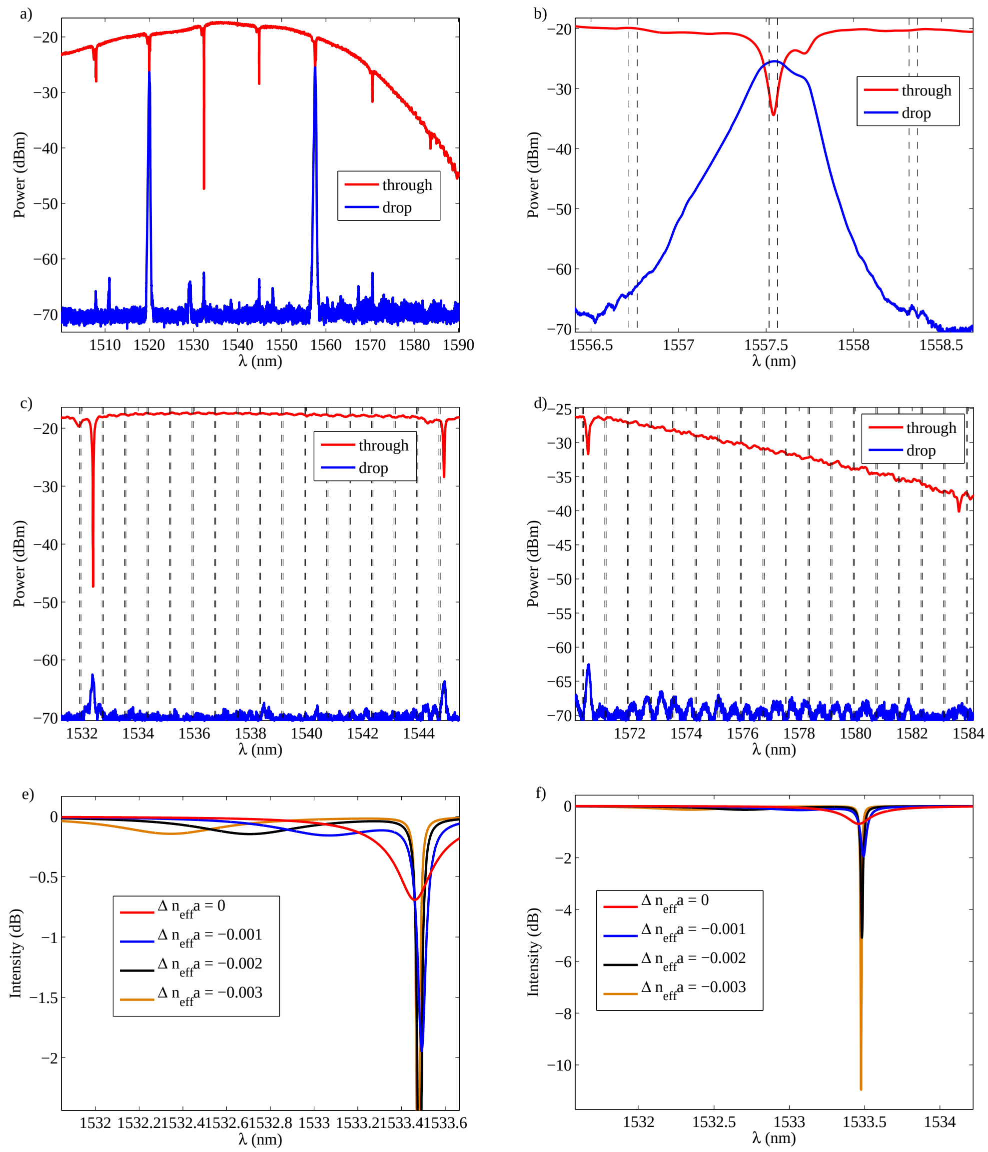

Fig. 3. (a) measured through port and drop port spectral response. (b) zoom-in of the measured major resonance. (c) zoom-in of the measured through port passband to the left of the major peak. (d) zoom-in of the measured through port passband to the right of the major peak. (e) zoom-in of the theoretical notch splitting when the effective index of racetrack resonator a decreases and (f) zoom-out of Fig. 3(e) (showing the increase in notch depth as the effective index of racetrack resonator a decreases).

#183816 - $15.00 USD Received 28 Jan 2013; revised 25 Mar 2013; accepted 27 Mar 2013; published 4 Apr 2013

Table 2. Experimental and Target Specifications

Parameter	Experimental	Target
FSR (nm)	37.52	$\geq$ 35.89
A_i (dB)	37.2	$\geq$ 25 [29, 30], 30 [31]
nA_i, IPS (dB)	39.7	$\geq$ 35 [31], 40 [29, 30]
R_{depth} (dB)	0.2	$\leq$ 0.5 [30]
EC_i (dB)	10.2	$\geq$ 10 [30], 12 [29]

4. Summary

In summary, we have experimentally shown that it is possible to meet numerous commercial requirements for dense wavelength-division multiplexing filters using quadruple series-coupled racetrack resonators exhibiting the Vernier effect. We have demonstrated a Vernier filter having a free spectral range greater than the span of the C-band (37.52 nm), a ripple of 0.2 dB, an adjacent channel isolation of 37.2 dB, an interstitial peak suppression of 39.7 dB, and an express channel isolation of 10.2 dB.

Appendices

Appendix: Quadruple series-coupled racetrack resonator transfer functions

Here, we will derive the drop port and through port transfer functions of quadruple series-coupled racetrack resonators using Mason's rule [40]. In [5], Dey *et al.* derived the drop port transfer function using Mason's rule [40] but did not derive nor present the through port transfer function. For completeness, here we have re-derived the drop port transfer function as well as derived the through port transfer function. Since in our configuration, there are four racetrack resonators coupled in series, there are 33 loop gains. There are 10 loop gains of the 10 possible combinations of 1 non-touching loop,

$$P_{11} = t_1 t_2 X_a, \tag{1}$$
$$P_{21} = t_2 t_3 X_b, \tag{2}$$
$$P_{31} = t_3 t_4 X_c, \tag{3}$$
$$P_{41} = t_4 t_5 X_d, \tag{4}$$
$$P_{51} = \kappa_2^2 \kappa_3^2 t_1 t_4 X_a X_b X_c, \tag{5}$$
$$P_{61} = \kappa_3^2 \kappa_4^2 t_2 t_5 X_b X_c X_d, \tag{6}$$
$$P_{71} = -\kappa_3^2 t_2 t_4 X_b X_c, \tag{7}$$
$$P_{81} = -\kappa_4^2 t_3 t_5 X_c X_d, \tag{8}$$
$$P_{91} = -\kappa_2^2 \kappa_3^2 \kappa_4^2 t_1 t_5 X_a X_b X_c X_d, \tag{9}$$
$$P_{101} = -\kappa_2^2 t_1 t_3 X_a X_b \tag{10}$$

where $X_{a,b,c,d} = exp(-\alpha_{a,b,c,d} L_{a,b,c,d} - j\beta_{a,b,c,d} L_{a,b,c,d})$, where the field loss coefficients and propagations constants for the racetrack resonators are represented by $\alpha_{a,b,c,d}$, and $\beta_{a,b,c,d}$, respectively. κ_1, κ_2, κ_3, κ_4, and κ_5 are the symmetric (real) point field coupling factors. t_1, t_2, t_3, t_4, and t_5 are the straight through (real) point field transmission factors. There are 15 loop gains of the 15 possible combinations of 2 non-touching loops,

$$P_{12} = P_{11}P_{21}, \tag{11}$$
$$P_{22} = P_{21}P_{31}, \tag{12}$$
$$P_{32} = P_{31}P_{41}, \tag{13}$$
$$P_{42} = P_{11}P_{31}, \tag{14}$$
$$P_{52} = P_{11}P_{41}, \tag{15}$$
$$P_{62} = P_{21}P_{41}, \tag{16}$$
$$P_{72} = P_{41}P_{51}, \tag{17}$$
$$P_{82} = P_{11}P_{71}, \tag{18}$$
$$P_{92} = P_{41}P_{71}, \tag{19}$$
$$P_{102} = P_{81}P_{101}, \tag{20}$$
$$P_{112} = P_{31}P_{101}, \tag{21}$$
$$P_{122} = P_{41}P_{101}, \tag{22}$$
$$P_{132} = P_{11}P_{81}, \tag{23}$$
$$P_{142} = P_{21}P_{81}, \tag{24}$$
$$P_{152} = P_{11}P_{61}. \tag{25}$$

There are 7 loop gains of the 7 possible combinations of 3 non-touching loops,

$$P_{13} = P_{11}P_{21}P_{31}, \tag{26}$$
$$P_{23} = P_{21}P_{31}P_{41}, \tag{27}$$
$$P_{33} = P_{31}P_{41}P_{101}, \tag{28}$$
$$P_{43} = P_{11}P_{41}P_{71}, \tag{29}$$
$$P_{53} = P_{11}P_{21}P_{81}, \tag{30}$$
$$P_{63} = P_{11}P_{21}P_{41}, \tag{31}$$
$$P_{73} = P_{11}P_{31}P_{41}. \tag{32}$$

There is 1 loop gain of the 1 possible combination of 4 non-touching loops,

$$P_{14} = P_{11}P_{21}P_{31}P_{41}. \tag{33}$$

The gain and co-factor of the first forward path that is used to determine the drop port transfer function is,

$$G_1 = -i\kappa_1\kappa_2\kappa_3\kappa_4\kappa_5\sqrt{X_aX_bX_cX_d}, \tag{34}$$
$$\Delta_1 = 1. \tag{35}$$

The determinant for the entire system is given by,

$$\begin{aligned}\Delta = 1 - &(P_{11}+P_{21}+P_{31}+P_{41}+P_{51}+P_{61}+P_{71}+P_{81}+P_{91}+P_{101})+\\ &(P_{12}+P_{22}+P_{32}+P_{42}+P_{52}+P_{62}+\\ &P_{72}+P_{82}+P_{92}+P_{102}+P_{112}+P_{122}+P_{132}+P_{142}+P_{152})-\\ &(P_{13}+P_{23}+P_{33}+P_{43}+P_{53}+P_{63}+P_{73})+P_{14}.\end{aligned} \tag{36}$$

Thus, the transfer function for the drop port is given by [5],

$$G_{drop} = \frac{G_1\Delta_1}{\Delta}. \tag{37}$$

#183816 - $15.00 USD Received 28 Jan 2013; revised 25 Mar 2013; accepted 27 Mar 2013; published 4 Apr 2013

The gains of the second to sixth forward path that are used to determine the through port transfer function are,

$$G_2 = t_1, \tag{38}$$

$$G_3 = -\kappa_1^2 t_2 X_a, \tag{39}$$

$$G_4 = \kappa_1^2 \kappa_2^2 t_3 X_a X_b, \tag{40}$$

$$G_5 = -\kappa_1^2 \kappa_2^2 \kappa_3^2 t_4 X_a X_b X_c, \tag{41}$$

$$G_6 = \kappa_1^2 \kappa_2^2 \kappa_3^2 \kappa_4^2 t_5 X_a X_b X_c X_d, \tag{42}$$

and the corresponding co-factors are,

$$\Delta_2 = \Delta, \tag{43}$$

$$\begin{aligned}\Delta_3 = 1 &- (P_{21} + P_{31} + P_{41} + P_{61} + P_{71} + P_{81}) \\ &+ (P_{22} + P_{32} + P_{62} + P_{92} + P_{142}) - P_{23},\end{aligned} \tag{44}$$

$$\Delta_4 = 1 - (P_{31} + P_{41} + P_{81}) + P_{32}, \tag{45}$$

$$\Delta_5 = 1 - P_{41}, \tag{46}$$

$$\Delta_6 = 1. \tag{47}$$

Thus, the transfer function for the through port is given by,

$$G_{through} = \frac{G_2\Delta_2 + G_3\Delta_3 + G_4\Delta_4 + G_5\Delta_5 + G_6\Delta_6}{\Delta}. \tag{48}$$

Acknowledgments

We would like to thank the Natural Sciences and Engineering Research Council of Canada for partial support of this project. Also, we wish to thank Lumerical Solutions, Inc., for providing the numerical software MODE Solutions. Part of this work was conducted at the University of Washington Microfabrication Facility, a member of the NSF National Nanotechnology Infrastructure Network. We would also like to thank Yun Wang for the design of the grating couplers.